JACS
JOURNAL OF THE AMERICAN CHEMICAL SOCIETY

ARTICLE

pubs.acs.org/JACS

Following Radical Pair Reactions in Solution: A Step Change in Sensitivity Using Cavity Ring-Down Detection

Kiminori Maeda,[†,‡,∥] Simon R. T. Neil,[§,∥] Kevin B. Henbest,[†,‡] Stefan Weber,[⊥] Erik Schleicher,[⊥] P. J. Hore,[§] Stuart R. Mackenzie,[*,§] and Christiane R. Timmel[*,†,‡]

[†]Department of Chemistry, University of Oxford, Inorganic Chemistry Laboratory, Oxford, OX1 3QR, U.K.

[‡]Centre for Advanced Electron Spin Resonance, University of Oxford, OX1 3QR, U.K.

[§]Department of Chemistry, University of Oxford, Physical and Theoretical Chemistry Laboratory, Oxford, OX1 3QZ, U.K.

[⊥]Institut für Physikalische Chemie, Albert-Ludwigs-Universität Freiburg, Albertstraße 21, 79104 Freiburg, Germany

ABSTRACT: The study of radical pair intermediates in biological systems has been hampered by the low sensitivity of the optical techniques usually employed to investigate these highly reactive species. Understanding the physical principles governing the spin-selective and magneto-sensitive yields and kinetics of their reactions is essential in identifying the mechanism governing bird migration, and might have significance in the discussion of potential health hazards of electromagnetic radiation. Here, we demonstrate the powerful capabilities of optical cavity-enhanced techniques, such as cavity ring-down spectroscopy (CRDS) in monitoring radical recombination reactions and associated magnetic field effects (MFEs). These include submicrosecond time-resolution, high sensitivity (baseline noise on the order of 10^{-6} absorbance units) and small (μL) sample volumes. Combined, we show that these represent significant advantages over the single-pass flash-photolysis techniques conventionally applied. The studies described here focus on photoinduced radical pair reactions involving the protein lysozyme and one of two possible photosensitizers: anthraquinone-2,6-disulphonate and flavin mononucleotide. CRDS-measured MFEs are observed in pump-probe experiments and discussed in terms of the sensitivity gains and sample-volume minimization afforded by CRDS when compared with flash photolysis methods. Finally, CRDS is applied to an in vitro MFE study of intramolecular electron transfer in the DNA-repair enzyme, *Escherichia coli* photolyase, a protein closely related to cryptochrome which has been proposed to mediate animal magnetoreception.

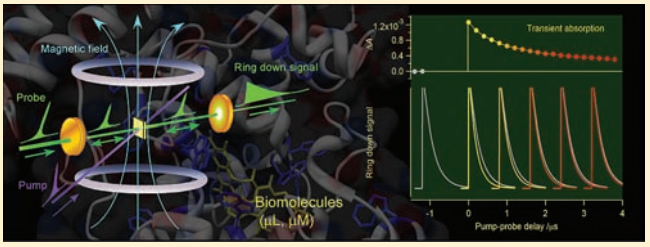

INTRODUCTION

Spin-correlated radical pairs (RPs), short-lived intermediates in a myriad of photolytic, thermolytic and radiolytic reactions, have been studied widely for over 40 years (reviewed in refs 1−3). It is well established that the application of external magnetic fields, either static or oscillating, can significantly affect the outcome of reactions proceeding via radical pairs by perturbing the kinetics and thus the yields of particular reaction paths. This fact, at first, seems surprising as the typical interaction energies are negligible compared to thermal energies. However, the physical origins of these field effects are well understood within the framework of the radical pair mechanism (RPM).[4] In this model, the radical pair is formed from a molecular precursor under conservation of total spin angular momentum and subsequently undergoes coherent evolution between its singlet and triplet electron-spin states. The efficiency of the singlet−triplet mixing process is determined by interactions of the radicals with both surrounding magnetic nuclei and externally applied magnetic fields. Spin-selective recombination from the singlet and triplet states of the pair can then lead to magnetosensitivity of the reaction yield if singlet and triplet channels lead to different products, or of the kinetics if recombination from the two states occurs at different rates.

The possibility that magnetic fields comparable with that of the Earth might affect reactions proceeding via radical pairs has attracted considerable attention in recent years, following the proposition that the RPM acts as the magnetoreception mechanism in migratory birds.[5,6] However, to date, only one experimental study has shown a true Earth-field effect, in a model system consisting of covalently linked fullerene, porphyrin and carotenoid moieties.[7] The discovery of cryptochrome, a blue-light receptor protein found in a variety of plants and animals including migratory birds, and the proposal of its role as a magnetoreceptor molecule,[5] has triggered an active search for any role it might play in magnetoreception. Thus far, no magnetic field-response of this system in vitro has been reported. Encouragingly, however, significant magnetic field effects (MFEs) have recently been reported on the photoinduced electron transfer reaction of *E. coli* photolyase (*Ec*PL), a closely related blue-light active enzyme of the same family.[8]

The vast majority of MFE studies has been based on optical spectroscopy. Photoemission measurements from radical pair products are widely used in both photochemistry[9−12] and radiation

Received: July 27, 2011
Published: September 20, 2011

chemistry[13−17] and represent highly sensitive, zero-background approaches. Direct optical absorption measurements, initiated by laser flash photolysis, have also been widely employed[1,18−22] and have the significant advantage that the radical pair products need not fluoresce or phosphoresce. However, conventional absorption spectroscopy is typically less sensitive than emission spectroscopy and often requires strong laser pulse irradiation to generate detectable radical concentrations, which in turn accelerates photodegradation.

Most time-resolved, in vitro MFE studies of biological molecules performed to date have employed laser flash photolysis.[23−25] Such studies, however, are severely hindered by the need for concentration and volume combinations far larger than practicable for most biological samples. Low concentrations and small solution volumes are associated with small signals in conventional transient absorbance (TA) studies. To some extent these can be offset by increasing the photoexcitation pulse energy, but photodegradation typically scales greater than linearly with laser intensity. It has become clear that a step change in methodology is required to extend MFE studies beyond model systems to biomolecular systems of interest.

Here we report the development of novel optical cavity-based techniques, based on cavity ring-down spectroscopy (CRDS),[26,27] which achieve sensitivity gains by increasing the path-length (via multiple passes) of light through an intracavity sample. In CRDS, a pulse of light (typically from a laser source) is injected into a high-finesse optical cavity and the time-constant describing the exponential decay of light circulating within the cavity (the ring-down time, τ), is measured. By its very nature, τ reflects the total optical losses per round-trip in the cavity, including the absorbance of any intracavity sample.[27] CRDS was conceived in and (largely) developed for the gas phase.[26] However, many of the same advantages are applicable in the condensed phase where it is gaining popularity.[28]

We have demonstrated previously highly sensitive MFE measurements using the combination of an optical cavity and magnetic field modulation via phase-sensitive detection.[29] A minimum detectable absorbance on the order of 10^{-5} per pass was demonstrated for the transient radical analyte and, when coupled with phase-sensitive detection, MFE-induced absorbance changes of $\sim 10^{-6}$ could be detected. However, such modulation-based approaches preclude acquisition of any temporal information on the transient species, such as their reaction kinetics.

Relatively few CRDS studies of solution reaction kinetics have been reported[30,31] and, of these, only Alexander, in a kinetic study of nitrate radical reactions with terpenes, has demonstrated sufficient temporal resolution to study transient radical species in solution using a flash-photolysis-based approach.[30] In this case the kinetics occurred on a time scale comparable with the ring-down time itself and were extracted by fitting the ring-down decay profiles.

Here we describe time-resolved CRDS measurements of photoinduced reactions, and their MFEs, in solution. Two model systems are studied and the results compared with those of conventional transient absorption measurements. Finally, we demonstrate the applicability of this approach to an in vitro MFE study of *E. coli* DNA photolyase. The technique, a pump-probe method with CRDS detection, uses varying pump-probe delay times to build up a temporal profile of the absorbing molecules and is particularly useful in detecting relatively short-lived species. It is thus complementary to other optical approaches for studying MFEs.

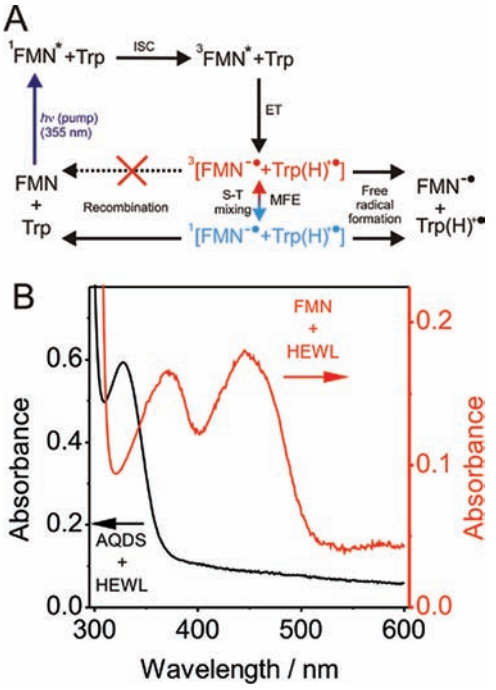

Figure 1. (A) Photochemical reaction scheme for the FMN, HEWL system; the reaction scheme for AQDS, HEWL is analogous (replace FMN with AQDS in the scheme). (B) UV−vis absorption spectra of 10 μM FMN, 0.5 mM HEWL (red line) and 0.1 mM AQDS, 0.1 mM HEWL (black line) in aqueous solution.

EXPERIMENTAL SECTION

Materials. The sodium salts of flavin mononucleotide (riboflavin-5′-monophosphate, referred to as FMN), and anthraquinone-2,6-disulphonate, referred to as AQDS), and hen egg white lysozyme (HEWL), were used as supplied (Sigma-Aldrich). A mutant of *E. coli* photolyase (*Ec*PL) that does not bind the methenyltetrahydrofolate (MTHF) cofactor was used, the expression and purification methods are described elsewhere.[32] The sample was diluted using a 50/50 (v/v) glycerol/water mixture, to give an *Ec*PL concentration of ~60 μM (vide infra). The non MTHF-binding mutant was used to minimize sample heterogeneity and photodegradation.[8] All solutions were made up using ultrapure water (Milli-Q, resistivity 18.2 MΩ cm, pH 6.3). The concentrations used for individual experiments are detailed later.

Photochemical Systems. *FMN and AQDS Systems.* Two closely related photochemical systems comprising lysozyme with one of two possible photosensitizers: FMN or AQDS were investigated in aqueous solution. The common photochemical scheme is shown in Figure 1A. Irradiation of the solution with UV light (355 nm, close to the ground-state absorption maxima of both FMN and AQDS, Figure 1B) generates the electronically excited substrate ^{1}FMN* (^{1}AQDS*). This then undergoes fast intersystem crossing (ISC) on the time scale of a few nanoseconds, to yield the excited triplet state, ^{3}FMN* (^{3}AQDS*). Subsequent electron transfer (ET), from a tryptophan (Trp) residue in lysozyme (most likely Trp123,[33] Trp62,[34] or both) to FMN/AQDS with conservation of total spin angular momentum, generates a triplet state radical pair, ^{3}[FMN$^{-\bullet}$ Trp(H)$^{+\bullet}$] or ^{3}[AQDS$^{-\bullet}$ Trp(H)$^{+\bullet}$], respectively.

In both systems, which conform to the RPM, the triplet-born RP can interconvert with the singlet state via singlet-triplet mixing induced by interaction of the electron spins with surrounding magnetic nuclei (Figure 1A). Importantly for these studies, the efficiency of this singlet-triplet mixing process may be affected significantly by applied magnetic fields. Upon radical re-encounter, only the singlet RP may recombine to

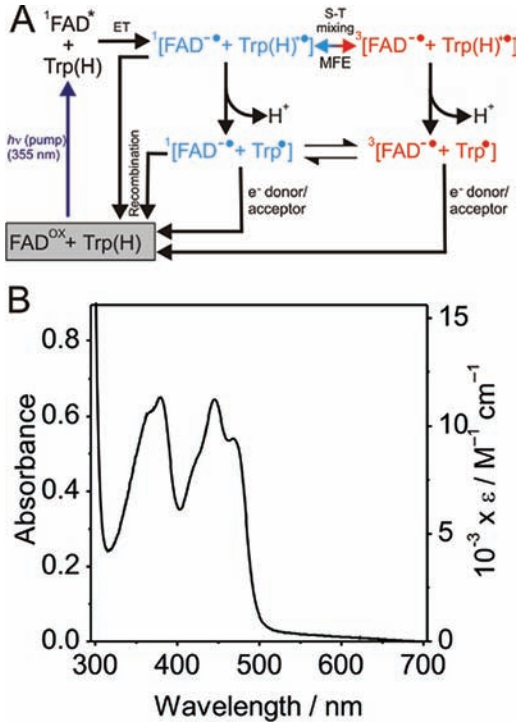

Figure 2. (A) Photochemical reaction scheme for the *Ec*PL system (see text for details). (B) UV−vis absorption spectrum of *Ec*PL: molar extinction coefficients, ε, are estimated by scaling the measured absorbance to the known FAD extinction coefficient (11200 M^{-1} cm^{-1}) at 443 nm.[35] The *Ec*PL concentration is thus estimated to be 60 μM.

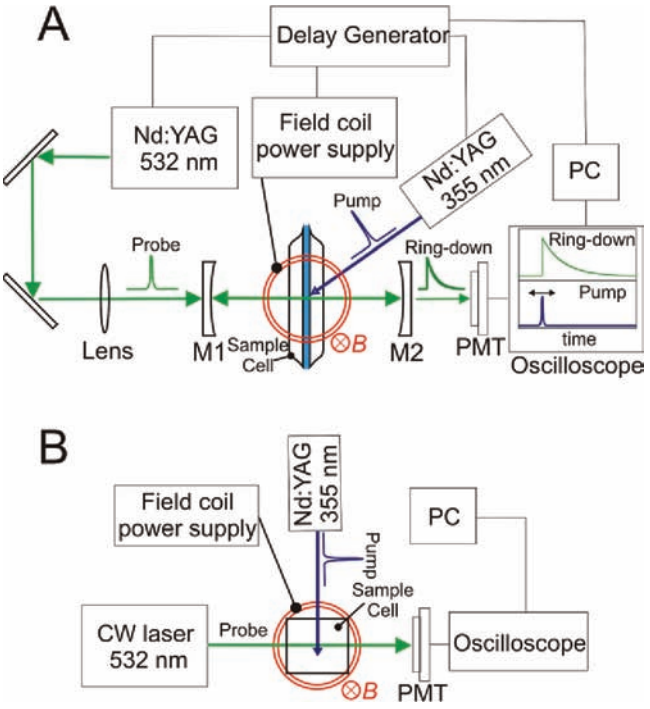

Figure 3. Schematics of the experimental CRDS (A) and TA (B) apparatus used to study radical concentration as a function of time and applied magnetic field strength. Helmholtz coils, indicated by concentric circles generate a static field, *B*, at the sample cell.

form the molecular precursor; the triplet RP is unreactive. As a result, the total radical yield is magnetic field-sensitive. In the experiments reported here, both CRDS and TA were used to monitor the radical concentration as a function of (i) applied magnetic field and (ii) pump-probe delay. A broad absorption band peaking around 520 nm and assigned to the photosensitizer radical, allows selective detection of the radicals present using a 532 nm Nd:YAG laser, while minimizing overlap with the ground state species.

EcPL System. A photochemical scheme devised by Henbest et al.,[8] describing radical pair formation and decay in *Ec*PL, is shown in Figure 2. Photoexcitation of the flavin adenine dinucleotide (FAD) cofactor in *Ec*PL in its fully oxidized redox state, FAD^{ox}, produces a singlet excited state (^{1}FAD*). ^{1}FAD* is then rapidly reduced (on a picosecond time scale), via cascade electron transfer along a chain of three tryptophan residues,[35−38] generating a RP, which, because of conservation of spin angular momentum, must be formed with the same spin multiplicity as its precursor. This singlet-born RP, $^1[FAD^{-\bullet}\ Trp(H)^{+\bullet}]$ may either recombine to form its ground state precursor, interconvert to the triplet state RP, $^3[FAD^{-\bullet}\ Trp(H)^{+\bullet}]$, or react with external electron acceptors/donors. Singlet-triplet interconversion, together with competition between RP recombination and Trp cation radical deprotonation, confers magnetic field sensitivity on the radical yield.

CRDS. The CRDS experiment is shown schematically in Figure 3A. A simple optical cavity is formed by two high-reflectivity mirrors, M1 and M2 (Layertec, broad-band coated, reflectivity $R_{532nm} = 0.9993$, radius of curvature 1 m) mounted 60 cm apart. Two different intracavity sample cells are used (Starna 45/Q, or Hellma 165−1.0−40) both of which have sample path lengths $l = 1$ mm. The Starna cell is used for the FMN (AQDS), HEWL experiments in which the (room temperature) sample flowed at 1 mL hr^{-1}. The Hellma sample cell is specifically designed for sample temperature control, via a glass jacket contacting the sample, through which coolant flowed. This cell is used for the *Ec*PL studies which are performed on a static sample at a temperature of −5 °C.

In all cases, the sample cell is oriented with its windows normal to the cavity axis using a goniometer stage. This geometry proves preferable to a Brewster's angle arrangement,[29] provided the cell has good optical surfaces. The sample cell is positioned at the center of the cavity between a pair of Helmholtz coils which provide the magnetic field. The photoexcitation (pump) pulse (355 nm, ∼7 ns, 10 Hz, Continuum Surelite I Nd:YAG laser) is directed through the sample as shown in Figure 3A. The CRDS (probe) pulse at 532 nm (5 ns, 10 Hz) is provided by a Continuum Minilite I Nd:YAG laser. Light exiting the cavity via the rear mirror (M2, Figure 3A) is detected by a photomultiplier tube (PMT, Hamamatsu, H6780), recorded on a digital oscilloscope (LeCroy Wavesurfer 42Xs, 2.5 GS s^{-1}, 400 MHz) and the data transferred to a personal computer (PC). The ring-down time, τ, is determined by a linear least-squares curve-fitting routine in IGOR Pro (Wavemetrics). From the ring-down times recorded with, τ, and without, τ_0, photoexcitation, the change in the per-pass absorbance, ΔA (on the conventional $\log_{10}$ scale), is calculated using

$$2.3026\Delta A = \frac{\tau_0 - \tau}{\tau_0 \tau}\left(\frac{L}{c}\right) \quad (1)$$

where L is the length of the cavity and c the speed of light.

Alignment of the pump beam path is achieved trivially via optimization of the CRDS-measured absorbance change within the sample cell. In order to build up the temporal evolution of the intracavity absorbance, a PC-controlled delay generator (SRS, DG535) is used to vary, in random order, between specified limits, the delay time (t_d) between pump and probe pulses. Variation of the magnetic field strength is achieved in a similar random fashion, via the power supply of the Helmholtz coils. All measurements are made at 10 Hz, with the exception of the *Ec*PL studies, in which the pump and probe pulses are operated at 1 Hz to allow for

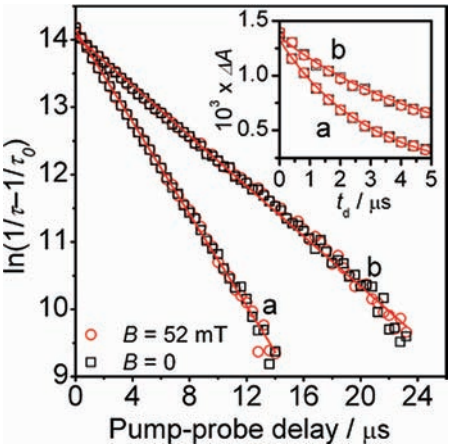

Figure 4. Kinetic study of the triplet excited state of FMN following photoexcitation (355 nm, pulse energy 0.6 mJ) of (a) unpurged (in ambient air) and (b) Ar-purged aqueous solution of 0.1 mM FMN. Points represent the experiments in the presence (red circles) and absence (black squares) of a 52 mT applied magnetic field, respectively. The inset displays the decay in the absorbance change at short pump-probe delays, on a linear scale. Each data point represents a 100-shot average. Solid red lines signify fits of the decay profiles to single exponential decays.

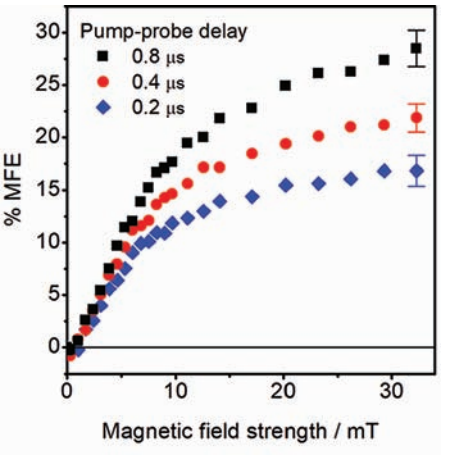

Figure 5. Percentage magnetic field effects (eq 4) as a function of magnetic field strength for a photoexcited aqueous solution of 0.1 mM AQDS and 0.1 mM HEWL measured by CRDS for various pump-probe delay times. Data points represent 500-shot averages. MFE traces are acquired with a 50-shot average per point: each MFE graph shown is the average of 10 such traces, the standard deviation of which is displayed at one data point, as a representative uncertainty. The field effects and their time dependence are consistent with those observed by Maeda et al.[25]

reoxidation of the flavin cofactor by dissolved dioxygen between laser shots.

Transient Absorption Measurements. The experimental setup for TA measurements is shown schematically in Figure 3B. The sample flows through a Hellma flow cell mounted between Helmholtz coils. The photoexcitation beam (Continuum Surelite I Nd:YAG, 355 nm output, 10 ns pulse at 10 Hz) and the CW (continuous wave) probe beam (Laser Quantum, Torus, 532 nm) are directed through the sample cell at right angles to one another, with path lengths l = 2 mm and 10 mm, respectively. The probe beam intensity exiting the sample cell is monitored with a PMT (Hamamatsu R928) and used to determine the ($\log_{10}$ scale) absorbance.

RESULTS AND DISCUSSION

^{3}FMN* Quenching Kinetics. A major aim of this paper is to demonstrate how CRDS may be used to monitor sensitively the effect of an applied magnetic field on the kinetics of photo-induced reactions. However, it is useful to provide first a more general illustration of CRDS's ability to probe chemical kinetics in solution. For this purpose, the quenching of the triplet excited state of FMN (^{3}FMN*) has been studied. Photoexcitation of an aqueous solution of pure FMN results in the formation of ^{3}FMN*, whose absorption spectrum exhibits a peak around 670 nm.[39] The inset of Figure 4 shows the CRDS-measured absorbance recorded at 532 nm, on the extreme blue tail of the ^{3}FMN* absorption band, as a function of pump-probe delay, t_d. The time-base is built-up by varying the pump-probe delay time as described above. The decay in ^{3}FMN* absorbance is dominated by a combination of (i) nonradiative relaxation to the ground state, (ii) quenching by molecular oxygen, (iii) self-quenching with ground-state FMN, and (iv) triplet-triplet annihilation.[40−45] In these experiments, iii and iv are minimized by the use of low FMN concentrations (0.1 mM) and low laser pulse energies (0.6 mJ). As a result, the triplet decay may be treated as a first order process with the concentration of ^{3}FMN* decaying exponentially from its initial value $[^3\text{FMN}^*]_0$. Equation 1 may then be used to derive the expression for the measured ring-down time[46]

$$\ln\left(\frac{1}{\tau}-\frac{1}{\tau_0}\right) = \ln\left(\frac{cl\varepsilon[^3\text{FMN}^*]_0}{L}\right) - kt_d \qquad (2)$$

in which k is the pseudo-first-order rate constant for the decay of ^{3}FMN*, ε is the molar extinction coefficient and l the sample path length. In all experiments, a small constant offset was observed resulting from production of some unidentified, persistent photoproduct. This contribution was removed from the $\ln(1/\tau - 1/\tau_0)$ data prior to fitting.

Plots of $\ln(1/\tau - 1/\tau_0)$ versus the pump-probe delay time, are shown in Figure 4. As expected, these plots are linear (R^2 = 0.995−0.998) and, via eq 2, allow determination of k^{-1} for both Ar-purged and unpurged systems: (5.38 ± 0.05) μs and (2.93 ± 0.02) μs, respectively. These lifetimes are consistent with those determined elsewhere[24,40] and permit an estimation of the rate constant for oxygen quenching of $(1.57 \pm 0.02) \times 10^9$ M^{-1} s^{-1}, (assuming $[O_2] = 2.60 \times 10^{-4}$ M) in the unpurged solution; this agrees well with the previously reported value due to Lasser et al. $(1.7 \pm 0.4) \times 10^9$ M^{-1} s^{-1}.[40] Measurements were performed in the presence and absence of an applied magnetic field as a negative control; the lack of magnetic field dependence is clear from the data in Figure 4.

The intercepts of the plots in Figure 4 are used to calculate $[^3\text{FMN}^*]_0 = 2.2 \times 10^{-5}$ M assuming $\varepsilon(^3\text{FMN}^*) = 1.25 \times 10^3$ M^{-1} cm^{-1}, estimated from Grodowski et al.[39] These triplet yields (~20%) seem sensible in view of the values observed and calculated previously and justify the pseudo-first-order treatment above.[39]

Importantly, Figure 4 and its analysis demonstrate the application of CRDS to a kinetic study in the liquid phase, by varying the pump-probe delay time to build up a temporal absorbance profile. The temporal resolution of this approach is, in principle, limited only by the electronics used to create the delay and the

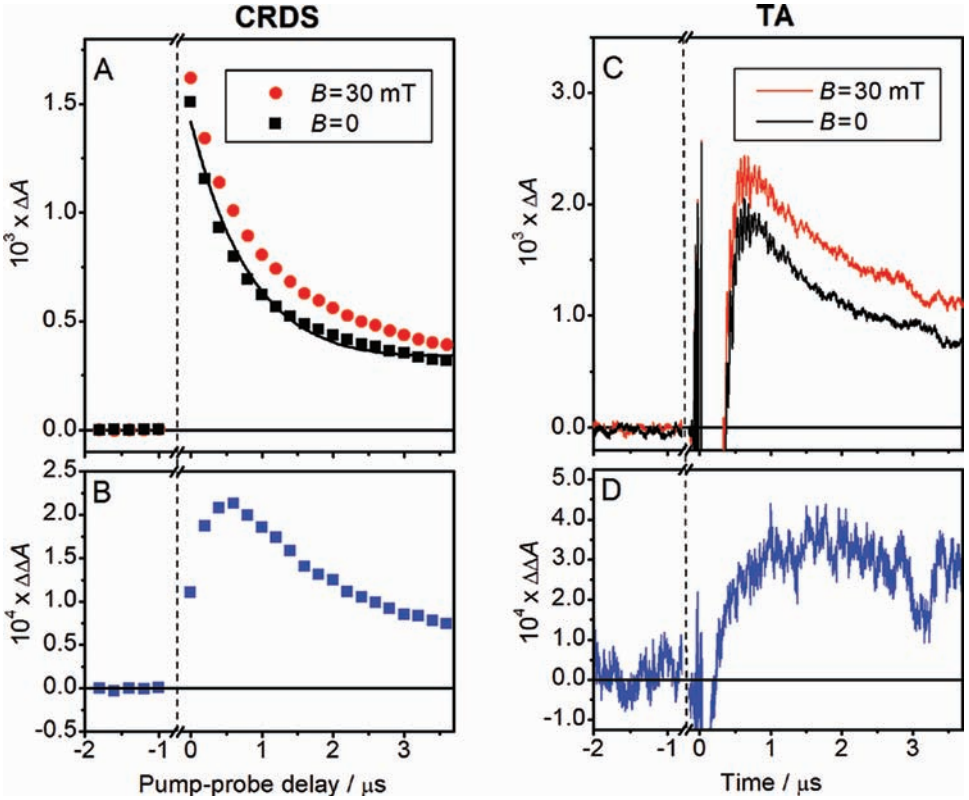

Figure 6. (A and C) Decay-time profiles of a photo excited aqueous solution of 0.1 mM AQDS and 0.1 mM HEWL in the presence (B = 30 mT, red) and absence (B = 0, black) of an applied magnetic field as measured by (A) CRDS (1 mJ photoexcitation pulse energy and 1 mm path length) and (C) TA (1 mJ photoexcitation pulse energy and 10 mm path length). The black line in A is a constrained double exponential fit to the B = 0 data (see text for details). (B and D) MFE time profiles $\Delta\Delta A(t)$ (= $\Delta A_{B=30\text{mT}} - \Delta A_{B=0}$), determined from the decay profiles, A and C, respectively. Note the difference in signal-to-noise between the CRDS and TA profiles. Note the breaks in the horizontal axes: CRDS data in the excluded range are corrupted by temporal overlap between the photoexcitation pulse and the ring-down decay.

pulse lengths of the light sources used. However, this method requires that the absorbance remains effectively constant over the ring-down times employed. As such, the lower limit of the temporal dynamic range may be taken as τ.[46] In these FMN studies, the range of τ is around 300−600 ns, which is still considerably shorter than the measured radical lifetimes (tens of microseconds). Kinetic information may be obtained from CRDS when the chemical decay rate is comparable to, or faster than, the ring-down rate, but extraction of the absolute absorbance requires fitting the data to more complex decay profiles.[30,47] Since the purpose of this article is to illustrate the use of CRDS in measuring MFEs, and to compare its performance with that of TA, we have not attempted this type of deconvolution. In this regard it is worth noting that (i) the user can to some extent control the ring-down time, without sacrificing the effective number of passes, via the length of the cavity, and (ii) radical pairs need to live for at least several hundred nanoseconds[48] to exhibit any sensitivity to the relatively weak magnetic fields (millitesla and below) of interest for the biological systems investigated here.

Under the experimental conditions employed, the upper limit of the temporal dynamic range is determined only by the time taken for the chemical decay to reach the minimum detectable change in absorbance, ΔA_{min}, which may be calculated as

$$\Delta A_{\text{min}} = \frac{\Delta\tau_{\text{min}} L}{2.3026 c \tau_0^2} \qquad (3)$$

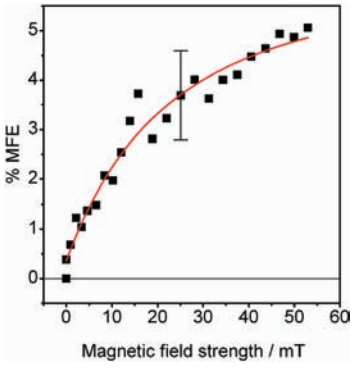

Figure 7. Percentage magnetic field effect (eq 4) as a function of magnetic field strength for an aqueous solution of 10 μM FMN and 0.5 mM HEWL using CRDS detection. The pump-probe delay time was held constant at 6 μs. MFE traces are acquired with a 200-shot average per point: the graph shown is the average of 10 such traces. The experimental uncertainty shown represents one standard deviation for an individual data point, and is representative of all points. The red line is included to guide the eye.

where $\Delta\tau_{\text{min}}$ is the minimum detectable change in the ring-down time. By way of example, in the ^{3}FMN* decay measurements (in Ar-purged solution), ΔA_{min} is determined as 2.8 × 10^{-6}, when $\Delta\tau_{\text{min}}$ = 0.8 ns is the standard deviation of the mean value of τ_0 over a 1 s period, during measurements on long time

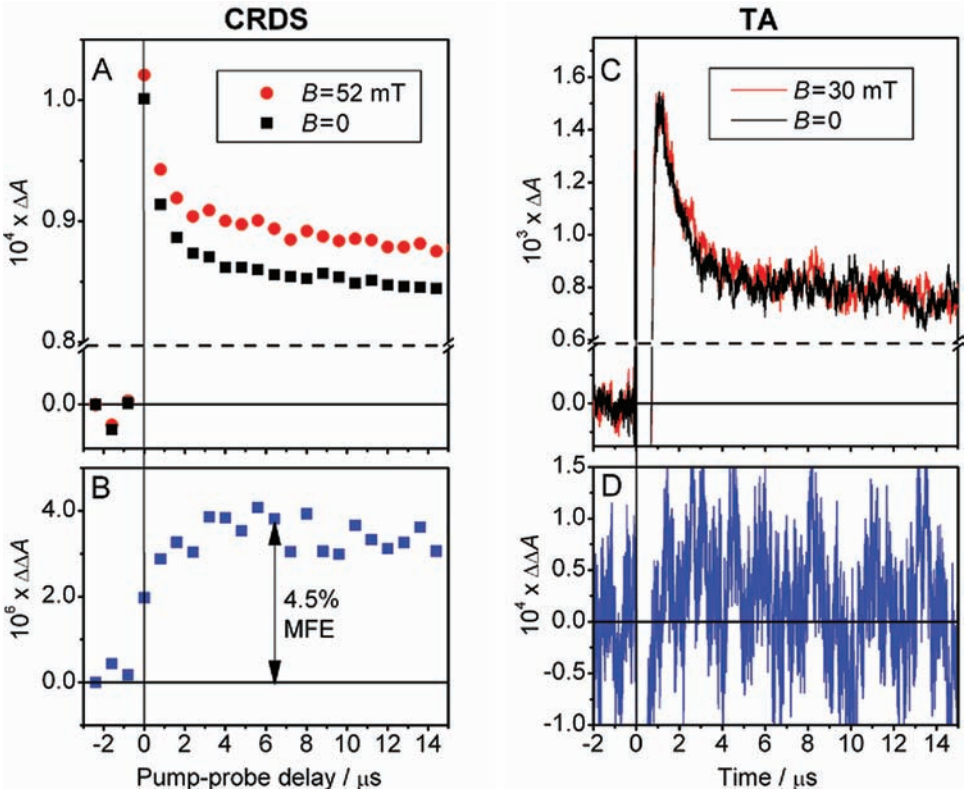

Figure 8. (A and C) Decay-time profiles of a photo excited aqueous solution of 10 μM FMN and 0.5 mM HEWL, measured by (A) CRDS (0.75 mJ pump pulse energy, 1 mm path length) and (C) TA (1 mJ pump pulse energy, 10 mm path length), in the presence and absence of an applied magnetic field (52 mT for CRDS and 30 mT for TA). (B and D) MFE time profiles $\Delta\Delta A(t)$ (= $\Delta A_B - \Delta A_{B=0}$), determined from decay profiles (A) and (C), respectively. Note the breaks in the vertical axes and the difference in $\Delta\Delta A(t)$ between CRDS and TA of roughly 2 orders of magnitude. All data points are 2000-shot averages.

scales (not shown here). The upper limit of the temporal dynamic range may be subsequently estimated as 32 μs, as determined from the time taken for ΔA to reach ΔA_{min}. It should be noted that, when identifying the upper temporal dynamic range limit, the time taken for the absorber to flow out of the detection volume must also be considered. In the example given above, this time is far longer than the ^{3}FMN* lifetime and, therefore, in this particular case, the temporal dynamic range is limited by the detection sensitivity and not the flow rate.

MFE on the AQDS, HEWL System. Having demonstrated the capabilities of our CRDS apparatus in studying simple solution-phase kinetics, we proceed to illustrate its applicability in the investigation of MFEs. Figure 5 displays the field-sensitive percentage change in the absorbance, ΔA, of the AQDS, HEWL system detected via CRDS at 532 nm in the absence (ΔA_0) and presence (ΔA_B) of a magnetic field according to

$$\%\text{MFE} = \frac{\Delta A_B - \Delta A_0}{\Delta A_0} \times 100 \qquad (4)$$

To facilitate comparison with a previously conducted TA-based study of this system, MFE graphs are plotted both as a function of pump-probe delay and magnetic field. As expected for a triplet-born radical pair, an increasing magnetic field produces a rise in the radical concentration (and hence %MFE) as the $T_{\pm1}$ spin levels become energetically more and more isolated from the S/T_0 manifold. The resulting drop in singlet-triplet interconversion efficiency leaves more radicals in the triplet state unable to recombine hence contributing strongly to the absorbance at 532 nm.

In satisfying agreement with previous reports,[25] the MFE for the early times rises most sharply between 2 and 10 mT while the MFE for the 0.8 μs pump-probe delay time is still not saturated at the highest field applied here. For the 0.2 μs delay data set, the magnetic field at which the MFE reaches half its maximum value $B_{1/2}$ = 8 mT, exceeds the theoretically predicted value[49] (4.5 mT) by a factor of nearly 2 indicating slow spin dynamics and the involvement of relaxation processes. Such behavior is typical for long-lived, triplet-born radical pairs in micelles or biradicals. As in previous TA studies,[25] the MFE graphs in Figure 5 contain contributions from radical pairs present throughout the ring-down time (250−350 ns for the AQDS, HEWL system). The uncertainty in the %MFE, determined from the standard deviation of 15 data points at 52 mT (1000-shot average per data point, data not shown), was found to be 0.8%, equivalent to a standard deviation in ΔA of 8×10^{-6}. This excellent signal-to-noise ratio (SNR) achieved for the MFE results from the large field effect observed in the AQDS system combined with the high sensitivity of the CRDS. The SNR is probably limited by two factors. First, the ring-down times correspond to only 60−90 cavity round trips per ring-down time, limited by scattering losses at the surface of, and within, the sample cell itself. Second, the scattering within the sample introduces measurement instability via fluctuations in the ring-down time. The ultimate sensitivity of the technique is discussed in more detail later.

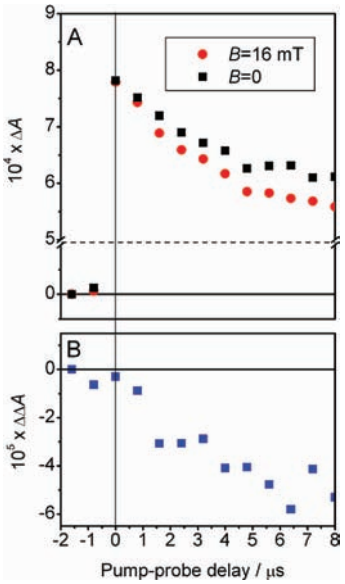

Figure 9. (A) Decay-time profiles for *Ec*PL, in the presence and absence of a 16 mT applied magnetic field as measured by CRDS (1 mJ pump pulse energy, 1 mm sample optical path length). Note the break in the vertical axis in (A). (B) MFE time profile, $\Delta\Delta A(t)$ ($= \Delta A_{B=16\mathrm{mT}} - \Delta A_{B=0}$), determined from the decay-time graph in (A). All data show 50-shot averages to minimize photodegradation.

The %MFE traces are useful in determining the initial spin state of the radical pair. In addition, the $B_{1/2}$ value permits identification of the radical pair and allows the investigation of exchange processes as a function of the concentration of the radical pair precursors.[50] Moreover, the %MFE traces determine whether a given system exhibits significant low field effects.[3] However, crucial parameters regarding the radical pair recombination and relaxation kinetics and their dependence on the magnetic field can only be obtained via time-resolved studies. Figure 6A demonstrates how CRDS can be used to monitor both the kinetics of RP decay and the effect of an external magnetic field on RP yield and decay kinetics. The figure shows the temporal profile of AQDS radical absorbance (in the AQDS, HEWL system), as a function of pump-probe delay, in the presence and absence of a 30 mT field. Each data point represents a 500-shot average. In both $B = 0$ and $B = 30$ mT cases, an initial rise in ΔA at pump-probe delay = 0, is followed by a nonexponential decay in absorbance. The rise in ΔA, because of RP generation, occurs within a few nanoseconds following photoexcitation[25] and is temporally unresolved. The decay of the absorbance comprises two components: a fast, strongly field-sensitive decay corresponding to geminate recombination of the RP and a slower component resulting from bulk recombination of free radicals. Previous work[25] has calculated the zero-field RP recombination rate constant, as $1.1 \times 10^6\ \mathrm{s}^{-1}$ (a 0.9 μs lifetime) and estimated the free radical decay lifetime between 5 and 16 μs. The relatively short time-base in Figure 6A prohibits fitting an unconstrained double-exponential decay. Fixing the time constants (0.9 and 5 μs) in a double-exponential fit produces the curve shown in the figure, with an acceptable root-mean-squared error of 3.8×10^{-5}, although this treatment should be viewed with caution, due to the second-order nature of free radical recombination kinetics. This is also a situation in which a more refined kinetic analysis would require a full deconvolution of ring-down time and radical pair kinetics.[30]

The real advantage of CRDS detection over TA becomes apparent in the measurement of the MFEs. Upon application of a magnetic field ($B = 30$ mT), there is a clear change in ΔA, which evolves in time as shown in Figure 6B. Following the initial increase in $\Delta\Delta A$, because of the field effect on RP recombination, the influence of (field-dependent) spin relaxation processes on recombination is observed, as $\Delta\Delta A$ decays in time: the complex kinetics of this system are described in detail elsewhere.[25]

Temporal profiles analogous to the CRDS measurements in Figure 6A and B have been recorded by TA and are shown in Figure 6C and D. Each profile in Figure 6C is a 2000-shot average. The noise on ΔA (and thus $\Delta\Delta A$) on the TA data ($\sim 10^{-4}$) is 2 orders of magnitude larger than in the CRDS experiments ($\sim 10^{-6}$). This reflects directly the increased optical path length through the sample in CRDS and the inherent insensitivity of CRDS to shot-to-shot intensity fluctuations in both the pump and probe beams. An additional advantage of CRDS is exemplified by the comparison of Figures 6A and 6C at early times (≤ 0.75 μs). During this time the TA detector is blinded by light scattered from the pump beam or fluorescence of the sample. CRDS, by contrast, is insensitive to such problems. Knowledge of the temporal evolution of the decay profile at early times is important when determining fitting parameters and hence CRDS has a distinct advantage over TA in this respect. Of course, a gated PMT (not available in this study) could go some way to removing the extent of interference seen in Figure 6C.

It is clear from the above that the sensitivity gain achieved in CRDS represents a major advantage over conventional TA. In turn, this sensitivity gain allows sample miniaturization: the sample volume probed in CRDS is estimated to be ~ 4 μL, a factor of 15 smaller than that in TA (~ 60 μL). Alternatively, CRDS permits the use of lower photoexcitation pulse energies than in TA. These attributes suggest CRDS will be well-suited to the study of biological samples, which can typically be produced only in microliter volumes, nano- to (a few) micromolar concentrations and which readily photodegrade. To demonstrate further the potential of CRDS in this field of interest, the biologically relevant model system, FMN, HEWL (described earlier), was studied, as described below.

MFE on the FMN, HEWL System. Figure 7 shows the %MFE as a function of field strength for the FMN, HEWL system. As for AQDS, HEWL, the field effect arises due to a decrease in S-T mixing efficiency and concomitant increase in the transient radical concentration. The MFE is, however, considerably smaller than that for AQDS, HEWL. In the latter, Coulombic interactions of the triply negatively charged AQDS radical with HEWL, which is positively charged at neutral pH (isoelectric point 11.4), extends the lifetime of the geminate radical pair promoting the evolution of significant magnetic field effects. By contrast, the relatively weak negative charge on the FMN radical results in a shorter geminate phase and hence a less pronounced field effect.

As a result, the field effect curve for the FMN, HEWL system is noisier than that shown in Figure 5, for AQDS. The MFE is still not saturated at the maximum field strength employed (52 mT) and the $B_{1/2}$ value is much larger than that predicted by theory (3 mT).[49] Again, this indicates slow spin dynamics in the system and the characteristic MFE can, therefore, be attributed to a combination of the hyperfine and spin relaxation mechanisms.

The decay kinetics in the FMN, HEWL system, measured by CRDS, in the presence and absence of an applied field, are shown in Figure 8A. As for AQDS, the FMN radical decay is observed as a

function of time and comprises fast (geminate recombination and excited triplet decay) and slow (free radical decay) components, in this case with respective time constants (0.60 ± 0.09) μs and (11 ± 7) μs, obtained from a double exponential fit to the $B = 0$ data in Figure 8A. The effect of applying the magnetic field is clear in Figure 8A and the difference profile (Figure 8B), even at the very low radical concentrations generated here: $\Delta\Delta A$ values of around 4×10^{-6} in Figure 8B correspond to changes in $[FMN^{-\bullet}]$ of 13 nM (assuming $\varepsilon_{532} = 3160\ M^{-1}\ cm^{-1}$).[51] The MFE at a pump−probe delay of 6.4 μs is calculated as 4.5%, close to the 5% effect shown in Figure 7 at the same field strength. The TA decay profiles, shown for comparison in Figure 8C, are qualitatively similar to those for CRDS. However, as illustrated in Figure 8D, under the conditions employed here, the effect of applying an external magnetic field is undetectable in the TA experiment. Note that the difference in applied field strength between TA and CRDS measurements (as necessitated by the coil geometries) is expected to produce slightly different %MFEs (4% MFE at 30 mT, compared with 5% at 52 mT). However, despite this and the associated effect on $\Delta\Delta A$, the superior SNR in CRDS is clear from a comparison of Figure 8B and D. The minimum detectable change in ΔA in TA (estimated from the standard deviation in $\Delta\Delta A$ over 100 data points around 4 μs, in Figure 8D) is $\sim 4.5 \times 10^{-5}$, from which the minimum detectable %MFE may be estimated as 5.3%. By contrast, 4.5% MFEs are easily observed using CRDS, even though the $\Delta\Delta A$ values measured are significantly smaller than in TA. As in the AQDS study, PMT blinding in the TA experiment prevents any useful data being extracted during the first microsecond after the pump pulse. From Figure 8 and the analysis above it is clear that the data obtained from CRDS are superior to that of TA.

MFEs in a Biological Sample: *Ec*PL. The decay kinetics in the *Ec*PL system, measured by CRDS, are shown in Figure 9A. The advantages of CRDS are clear: despite the small sample volume and low photoexcitation pulse energies used, changes in radical absorbance on the order of 10^{-5} are clearly observed. In contrast to the systems discussed above, the RP in *Ec*PL is born in the singlet state[8] and hence application of a magnetic field leads to an *increased* recombination efficiency and a net decrease in the transient radical concentration. A detailed analysis of the decay kinetics in this system will be published elsewhere but over the pump-probe delay range shown in Figure 9A the changes in absorbance are probably dominated by radical recombination from the primary radical pair (see Figure 2) with concomitant loss of $FAD^{-\bullet}$ and $Trp(H)^{+\bullet}$ radical absorption (with broad maxima at ~500 and 600 nm, respectively). A small additional contribution from conversion of $Trp(H)^{+\bullet}$ to $Trp^{\bullet}$ ($\lambda_{max} \approx$ 500 nm) in the secondary radical pair is also likely.[8]

By contrast with the earlier work of Henbest et al.,[8] in which ferricyanide was added to ensure rapid reoxidation of $FAD^{-\bullet}$ back to the FAD^{ox} precursor, in this work no external electron acceptor was added to the sample prior to the experiments. Additionally, only a minor fraction of $Trp^{\bullet}$ is thought to be reduced by an unknown external electron donor. Therefore, a very long reoxidation lifetime (17 ms) is expected in the secondary radical pair.[37] Although such a long decay component is not apparent in Figure 9A, the observation of a MFE, clear in Figure 9B, suggests that rapid reoxidation from the secondary RP is not necessary, as under the mild irradiation conditions used there is minimal conversion of the protein into its radical state. This is probably a direct result of the weak photoexcitation powers required using CRDS detection, again demonstrating the advantage of this technique over TA. The noise in $\Delta\Delta A$ shown in Figure 9B, for a 100 s measurement, is on the order of 10^{-5} and is currently limited by scattering within the *Ec*PL sample. Thus, it is feasible to believe that by carefully adjusting the *Ec*PL concentration and sample-cell path length, additional sensitivity gains may be achieved, permitting lower photoexcitation powers and/or measurement repetition-rates to be employed, thereby further reducing the risk of sample photodegradation.

CONCLUSIONS AND OUTLOOK

In summary, a pump-probe variant of CRDS allows the time-resolved study of photoinduced reactions and their MFEs in solution, with a detection sensitivity on the order of 10^{-6}, around 2 orders of magnitude smaller than that achieved with conventional TA. The sensitivity gains in CRDS allow a reduction in the probed sample volume (down to 4 μL, around an order of magnitude lower than in TA), facilitating low-volume biological-sample experiments. The significant advantages of CRDS have been demonstrated in proof-of-principle studies, using AQDS- and FMN-based systems and have been successfully applied to study MFEs in *Ec*PL, a biomolecule with a close similarity to cryptochrome.

Further reductions in the sample volume probed could be achieved by altering the cell design to reduce its dead volume. Alternatively, ultralow volume (nL) cavity-based techniques, such as fiberloop-[52] or evanescent wave-CRDS could be employed.[28] In future, we envision using broadband cavity-enhanced absorption spectroscopy[53] using intense supercontinuum light sources (now commercially available as turn-key systems) to monitor radical absorption and MFEs over wide wavelength ranges (hundreds of nanometers, covering entire absorption bands),[54,55] providing valuable spectral information for use in elucidating chemical reaction schemes, particularly in systems where multiple spectrally overlapping absorbing species may be present, such as in photolyase or cryptochrome.

AUTHOR INFORMATION

Corresponding Author

stuart.mackenzie@chem.ox.ac.uk; christiane.timmel@chem.ox.ac.uk

Author Contributions

‖These authors contributed equally.

ACKNOWLEDGMENT

Financial support for this research was provided by the Defense Advanced Research Projects Agency (QuBE: N66001-10-1-4061), the EMF Biological Research Trust (BRT 08/33 and BRT 10/36) and the Engineering and Physical Sciences Research Council (SRTN).

REFERENCES

(1) Steiner, U. E.; Ulrich, T. *Chem. Rev.* **1989**, *89*, 51–147.
(2) Woodward, J. R. *Prog. React. Kinet. Mech.* **2002**, *27*, 165–207.
(3) Timmel, C. R.; Henbest, K. B. *R. Soc. Lond. Phil. Trans.* **2004**, *362*, 2573–2589.
(4) Kaptein, R.; Oosterhoff, J. L. *Chem. Phys. Lett.* **1969**, *4*, 195–197.
(5) Ritz, T.; Adem, S.; Schulten, K. *Biophys. J.* **2000**, *78*, 707–718.
(6) Schulten, K.; Swenberg, C. E.; Weller, A. *Z. Phys. Chem.* **1978**, *111*, 1–5.

(7) Maeda, K.; Henbest, K. B.; Cintolesi, F.; Kuprov, I.; Rodgers, C. T.; Liddell, P. A.; Gust, D.; Timmel, C. R.; Hore, P. J. *Nature* **2008**, *453*, 387–390.
(8) Henbest, K. B.; Maeda, K.; Hore, P. J.; Joshi, M.; Bacher, A.; Bittl, R.; Weber, S.; Timmel, C. R.; Schleicher, E. *Proc. Natl. Acad. Sci. U. S. A.* **2008**, *105*, 14395–14399.
(9) Iwasaki, Y.; Murai, H.; Maeda, K.; Azumi, T. *Chem. Phys.* **1998**, *230*, 201–208.
(10) Iwasaki, Y.; Maeda, K.; Murai, H. *J. Phys. Chem. A* **2001**, *105*, 2961–2966.
(11) Henbest, K. B.; Maeda, K.; Athanassiades, E.; Hore, P. J.; Timmel, C. R. *Chem. Phys. Lett.* **2006**, 571–576.
(12) Henbest, K. B.; Athanassiades, E.; Maeda, K.; Kuprov, I.; Hore, P. J.; Timmel, C. R. *Mol. Phys.* **2006**, *104*, 1789–1794.
(13) Kalneus, E. V.; Stass, D. V.; Ivanov, K. L.; Molin, Y. N. *Mol. Phys.* **2006**, *104*, 1751–1763.
(14) Kalneus, E. V.; Kipriyanov, A. A.; Purtov, P. A.; Stass, D. V.; Molin, Y. N. *Dokl. Phys. Chem.* **2007**, *415*, 170–173.
(15) Kalneus, E. V.; Kipriyanov, A. A.; Purtov, P. A.; Stass, D. V.; Molin, Y. N. *Appl. Magn. Reson.* **2006**, *30*, 549–554.
(16) Sergey, N. V.; Burdukov, A. B.; Pervukhina, N. V.; Kuibida, L. V.; Pozdnyakov, I. P.; Stass, D. V. *Chem. Phys. Lett.* **2011**, *504*, 107–112.
(17) Usov, O. M.; Stass, D. V.; Tadjikov, B. M.; Molin, Y. N. *J. Phys. Chem. A* **1999**, *103*, 1690–1690.
(18) Turro, N. J.; Chow, M. F.; Chung, C. J.; Tanimoto, Y.; Weed, G. C. *J. Am. Chem. Soc.* **1981**, *103*, 4574–4576.
(19) Tanimoto, Y.; Takashima, M.; Itoh, M. *Chem. Phys. Lett.* **1983**, *100*, 442–444.
(20) Zimmt, M. B.; Doubleday, C.; Turro, N. J. *J. Am. Chem. Soc.* **1985**, *107*, 6726–6727.
(21) Hayashi, H.; Sakaguchi, Y.; Kamachi, M.; Schnabel, W. *J. Phys. Chem.* **1987**, *91*, 3936–3938.
(22) McLauchlan, K. A. *Appl. Magn. Reson.* **1996**, *11*, 357–373.
(23) Mohtat, N.; Cozens, F. L.; Hancock-Chen, T.; Scaiano, J. C.; McLean, J.; Kim, J. *Photochem. Photobiol.* **1998**, *67*, 111–118.
(24) Miura, T.; Maeda, K.; Arai, T. *J. Phys. Chem. B* **2003**, *107*, 6474–6478.
(25) Maeda, K.; Robinson, A. J.; Henbest, K. B.; Dell, E. J.; Timmel, C. R. *J. Am. Chem. Soc.* **2010**, *132*, 1466–1467.
(26) O'Keefe, A.; Deacon, D. A. G. *Rev. Sci. Instrum.* **1988**, *59*, 2544–2551.
(27) Berden, G.; Peeters, R.; Meijer, G. *Int. Rev. Phys. Chem.* **2000**, *19*, 565–607.
(28) Schnippering, M.; Neil, S. R. T.; Mackenzie, S. R.; Unwin, P. R. *Chem. Soc. Rev.* **2011**, *40*, 207–220.
(29) Neil, S. R. T.; Maeda, K.; Henbest, K. B.; Goez, M.; Hemmens, R.; Timmel, C. R.; Mackenzie, S. R. *Mol. Phys.* **2011**, *108*, 993–1003.
(30) Alexander, A. J. *Chem. Phys. Lett.* **2004**, *393*, 138–142.
(31) Hallock, A. J.; Berman, E. S. F.; Zare, R. N. *J. Am. Chem. Soc.* **2003**, *125*, 1158–1159.
(32) Schleicher, E.; Hessling, B.; Illarionova, V.; Bacher, A.; Weber, S.; Richter, G.; Gerwert, K. *FEBS J.* **2005**, *272*, 1855–1866.
(33) Kiryutin, A. S.; Morozova, O. B.; Kuhn, L. T.; Yurkovskaya, A. V.; Hore, P. J. *J. Phys. Chem. B* **2007**, *111*, 11221–11227.
(34) Hore, P. J.; Kaptein, R. *Biochemistry* **1983**, *22*, 1906–1911.
(35) Jorns, M. S.; Wang, B. Y.; Jordan, S. P.; Chanderkar, L. P. *Biochemistry* **1990**, *29*, 552–561.
(36) Aubert, C.; Mathis, P.; Eker, A. P. M.; Brettel, K. *Proc. Natl. Acad. Sci. U. S. A.* **1999**, *96*, 5423–5427.
(37) Aubert, C.; Vos, M. H.; Mathis, P.; Eker, A. P. M.; Brettel, K. *Nature* **2000**, *405*, 586–590.
(38) Lukacs, A.; Eker, A. P. M.; Byrdin, M.; Brettel, K.; Vos, M. H. *J. Am. Chem. Soc.* **2008**, *130*, 14394–14395.
(39) Grodowski, M. S.; Veyret, B.; Weiss, K. *Photochem. Photobiol.* **1977**, *26*, 341–352.
(40) Lasser, N.; Feitelson, J. *Photochem. Photobiol.* **1975**, *21*, 249–254.
(41) Levin, P. P.; Tatikolov, A. S.; Panova, I. G.; Sul'timova, N. B. *High Energy Chem.* **2010**, *44*, 216–219.
(42) Viteri, G.; Edwards, A. M.; De la Fuente, J.; Silva, E. *Photochem. Photobiol.* **2003**, *77*, 535–540.
(43) Gibson, Q. H.; Massey, V.; Atherton, N. M. *Biochem. J.* **1962**, *85*, 369–370.
(44) Song, P. S.; Moore, T. A.; Kurtin, W. E. *Z. Naturforsch.* **1972**, *B 27*, 1011.
(45) Mueller, F.; Mayhew, S. G.; Massey, V. *Biochemistry* **1973**, *12*, 4654–4662.
(46) Yu, T.; Lin, M. C. *J. Am. Chem. Soc.* **1993**, *115*, 4371–4372.
(47) Brown, S. S.; Ravishankara, A. R.; Stark, H. *J. Phys. Chem. A* **2000**, *104*, 7044–7052.
(48) Timmel, C. R.; Till, U.; Brocklehurst, B.; McLauchlan, K. A.; Hore, P. J. *Mol. Phys.* **1998**, *95*, 71–89.
(49) Weller, A.; Nolting, F.; Staerk, H. *Chem. Phys. Lett.* **1983**, *96*, 24–27.
(50) Justinek, M.; Grampp, G.; Landgraf, S.; Hore, P. J.; Lukzen, N. N. *J. Am. Chem. Soc.* **2004**, *126*, 5635–5646.
(51) Mueller, F.; Bruestlein, M.; Hemmerich, P.; Massey, V.; Walker, W. H. *Eur. J. Biochem.* **1972**, *25*, 573–580.
(52) Waechter, H.; Litman, J.; Cheung, A. H.; Barnes, J. A.; Loock, H. P. *Sensors* **2010**, *10*, 1716–1742.
(53) Fiedler, S. E.; Hese, A.; Ruth, A. A. *Rev. Sci. Instrum.* **2005**, *76*, 023107.
(54) van der Sneppen, L.; Hancock, G.; Kaminski, C.; Laurila, T.; Mackenzie, S. R.; Neil, S. R. T.; Peverall, R.; Ritchie, G. A. D.; Schnippering, M.; Unwin, P. R. *Analyst* **2010**, *135*, 133–139.
(55) Schnippering, M.; Unwin, P. R.; Hult, J.; Laurila, T.; Kaminski, C. F.; Langridge, J. M.; Jones, R. L.; Mazurenka, M.; Mackenzie, S. R. *Electrochem. Commun.* **2008**, *10*, 1827–1830.